INSTITUTE OF PHYSICS PUBLISHING PLASMA SOURCES SCIENCE AND TECHNOLOGY

Plasma Sources Sci. Technol. **15** (2006) 757–764 doi:10.1088/0963-0252/15/4/020

A Fabry–Pérot spectroscopy study on ion flow features in a Hall effect thruster

D Gawron[1,3], **S Mazouffre**[1] **and C Boniface**[2]

[1] Laboratoire d'Aérothermique, 1C avenue de la Recherche Scientifique, 45071 Orléans, France

[2] CPAT, CNRS, Université Paul Sabatier, 118 route de Narbonne, 31062 Toulouse, France

E-mail: gawron@cnrs-orleans.fr

Received 23 March 2006, in final form 7 July 2006
Published 25 August 2006
Online at stacks.iop.org/PSST/15/757

Abstract

The exit velocity of singly-charged xenon ions is determined by means of Fabry–Pérot interferometry at the exhaust of a high-power PPSX000 Hall effect thruster by analysing the Doppler shifted spectral profile of the 541.91 nm Xe^+ ion line. A technique combining numerical simulations and CCD imaging is used to re-adjust the obtained velocity profiles in space, as this information is lost due to the accumulation of light along the line of sight. The applied voltage is varied from 200 to 900 V, and the xenon mass flow rate is varied from 5 mg s^{-1} to 15 mg s^{-1} to investigate the evolution of both the ion speed and the distribution of the accelerating potential over a broad power range. The goal of these measurements is twofold, namely, collecting reliable and extensive data and looking for a simple correlation between thruster parameters and corresponding accelerating potential distributions. Furthermore, this study reveals the presence of low velocity ions in the vicinity of the thruster channel exhaust.

(Some figures in this article are in colour only in the electronic version)

1. Introduction

Electric propulsion (EP) has been available for more than 30 years. It was first developed in the Soviet Union for the mass propellant savings it allowed. Indeed, electric thrusters allow high specific impulse (I_{sp}) thanks to the acceleration of ionized propellant which reaches velocities much higher than in thermochemical thrusters. Several kinds of electric thrusters have already been developed, such as gridded ion engines, pulsed plasma thrusters and Hall effect thrusters (HET).

Within the EP technologies, HET inherit a long successful flight history from the Soviet/Russian space programme, which has flown the stationary plasma thruster (SPT) variant since 1972 [1]. HET implementation on Western satellites or space missions is now underway [1–3]. The interest in HET in space technology is related to several features of these thrusters:

(1) much higher specific impulse (>1400 s) in comparison with chemical thrusters (<500 s) with thrust efficiency ∼ 0.5, thrust level ∼100 mN, lifetime >5000 h at 1.5 kW electric power;

(2) relatively simple and robust design provides gridless acceleration of the ion flow;

(3) dual-mode operation, i.e. either high thrust or high I_{sp} regimes;

(4) significant input from previous experience.

Recent industrial development in Europe (Snecma and Astrium) [2], in the US (Busek, Aerojet and Pratt and Whitney) led to a revival in related research. Recent successes such as the SMART-1 spacecraft mission around the moon demonstrate that HET are good candidates for $I_{sp} < 2000$ s [4]. However, larger HET which would be both more powerful and versatile in their use could also be of interest for orbit transfer and station keeping of larger satellites. In this context, a prototype model of a high power HET with dual-mode capability called PPSX000 was developed by Snecma. The PPSX000 HET was designed to allow both high thrust (up to 400 mN) and high I_{sp} (up to 3000 s), the operating range being bounded by plasma discharge dynamics and thermal limitations [5].

HETs are based on so-called ion accelerators with closed electron drift. A discharge voltage U_d is applied between an

[3] Author to whom any correspondence should be addressed.

external cathode and an anode located at the bottom of an annular ceramic channel. Xenon (Xe) gas, which is used as a propellant, is fed through the anode and a complementary gas flow is required for the cathode operation. A set of coils provides a radial magnetic field whose strength is at its maximum near the channel exhaust. The magnetic field has to be strong enough to trap electrons around Larmor orbits, hence resulting in reduced longitudinal mobility in this area, leading in turn to a localized potential drop whose order of magnitude is U_d. The resulting $\boldsymbol{E} \times \boldsymbol{B}$ configuration leads to an electron drift in the azimuthal direction. The electron energy is typically higher than 10 eV, thus allowing efficient ionization of Xe atoms. Xe flow from the anode is typically ionized at ∼90%, allowing the resulting ions to be accelerated by the electric field. Therefore, the ions leaving the ceramic channel eventually reach kinetic energies whose order of magnitude corresponds to U_d.

Determination of the exhaust velocity of singly-ionized Xe in the HET plasma plume provides valuable information about the thruster operating conditions and overall performance. Indeed, the ion exit velocity determines the specific impulse and is directly linked to the thrust and thruster efficiency. Furthermore, the local plasma potential and electric field can be derived from a measurement of the ion velocity map. Laser induced fluorescence (LIF) spectroscopy is particularly suited to this study as it offers a set of matchless features in terms of spectral and spatial resolution. However, it is a cumbersome diagnostic tool that is not straightforward to implement in ground-test facilities dedicated to HET studies. Development of a non-intrusive diagnostic tool, which is less complicated to use than LIF spectroscopy, yet complementary in its contribution, is essential in order to perform investigations of Xe^+ ion flow characteristics, whatever the thruster geometry and operating conditions are. Fabry-Pérot (FP) interferometry, which is based on the analysis of light emitted by the plasma, fulfils these requirements although it lacks the spectral as well as spatial resolution of LIF spectroscopy. Nevertheless, FP interferometry measures the ion velocity with good accuracy over a range of thruster operating conditions, with greater ease and speed than LIF spectroscopy. Moreover, FP interferometry works simultaneously with far-field plume diagnostics. In this paper, we present measurements of the Xe^+ ion axial velocity realized within the plasma of a high-power laboratory-model PPSX000 HET by means of FP spectroscopy. All reported measurements have been carried out by studying the spectral profile of the $Xe^+ 5p^4(^3P_2)6s[2]_{3/2} \rightarrow 5p^4(^3P_2)6p[3]_{5/2}$ transition occurring at 541.91 nm. For the measurements presented in this article the thruster is operated with a U_d of 200 to 900 V, at Xe mass flow rates of 5 to 15 mg s^{-1}.

2. Experimental setup

A FP interferometer is a very narrow bandwidth optical filter. It is often used to examine the detailed structure of spectral lines [6,7]. Figure 1 presents a schematic view of the complete FP system. A lens collects light from the thruster xenon plasma. The light is then transported towards the optical bench by means of a multimode silica step index optical fibre with a 365 μm core diameter. A lens with a 400 mm focal distance collimates the light which exits the fibre into a beam. The

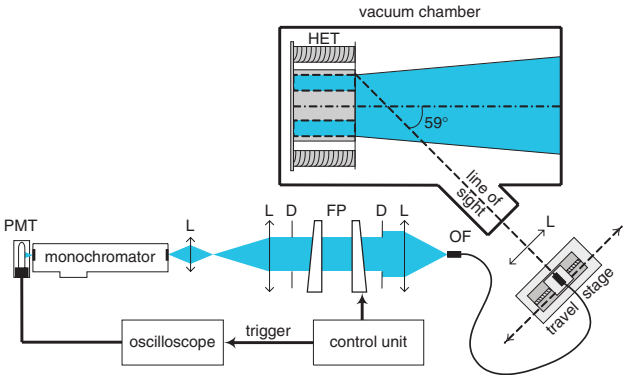

Figure 1. Fabry-Pérot Experimental setup (L: lens; D: diaphragm; OF: optical fibre).

parallel beam passes a plane FP cavity limited by two 2.5 cm diameter apertures. The cavity mirror coating is optimized for wavelengths ranging from 450 to 550 nm. Behind the cavity, the transmitted light is focused onto a 0.7 mm pinhole in order to solely select the central interference ring. The pinhole is imaged onto the entrance slit of a 40 cm monochromator that acts as a rough wavelength selector to separate the line to be studied from the remainder of the spectrum ($\Delta\lambda \sim$ 0.8 nm). A photomultiplier tube (Hamamatsu R928) is used as a light detector. The delivered signal is registered with an oscilloscope. The FP (RC110 from Burleigh) is a piezo-scanned type; the length as well as the alignment of the cavity is controlled by applying a high voltage onto piezoelectric mirror mounts. An accurate frequency scan is realized by smoothly varying the mirror position with a high voltage ramp. All measurements presented in this paper are obtained with a cavity scanning frequency of 10 Hz.

The distance between the two dielectric mirrors of the FP cavity is 3.0 mm, meaning that the free spectral range of the cavity is equal to 50.0 GHz [8]. In the spectral domain of interest ($\lambda \sim$ 540 nm) mirror reflectivity is around 0.953. The mirrors are flattened to $\lambda/200$. Therefore, the net finesse of the FP cavity is around 62. The instrumental finesse that characterizes the resolving power of the complete FP bench by accounting for pinholes and lenses induced losses is found to be around 59 [8]. In other words, the setup allows achieving a spectral resolution of about 0.75 GHz, i.e. 0.7 pm at 542 nm, as the light beam is perfectly collimated. The apparatus profile does not allow resolving the complex structure of the Xe^+ line; however, it is narrow enough to precisely measure the Doppler shift. The strong Ne I line at 540.06 nm, which is emitted by a low-pressure neon lamp, is used to accurately align the FP bench. The optical fibre, which collects light from the thruster is mounted onto a micrometric travel stage so that it moves in the focal plane of the collection lens, which has a focal length of 100 mm. This allows the line of sight of the detection branch to change without moving the thruster. For the results discussed in this article, the angle θ between the line of sight and the thruster axis is set to 59°. Note that the line of sight is contained in the horizontal plane that contains the symmetry axis of the thruster. The distance between the lens and the thruster is 1.70 m and the optical magnification is 17. Since the fibre radius is 365 μm, the detection branch collects photons inside a cylinder ∼6 mm in diameter. The distance

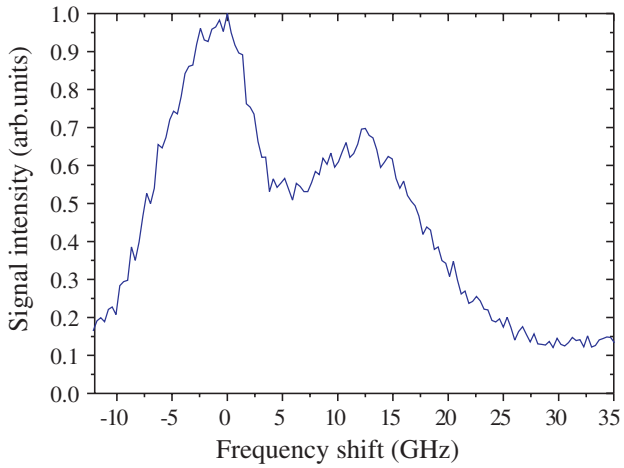

Figure 2. Typical interference pattern measured by Fabry–Pérot interferometry.

between the thruster and the lens is considered to be infinite so that it is not necessary to take the field depth into account for calculations (this has been verified experimentally).

Note that the facility backpressure varies from 2×10^{-5} to 7×10^{-5} mbar as the Xe mass flow rates is changed from 5 to 15 mg s^{-1}. A high quality of the facility vacuum is necessary to warrant no disturbance of the plasma properties and no change in thruster parameters like the thrust [9].

Figure 2 displays a 541.9 nm Xe^+ line interference pattern obtained with this set-up in the plasma plume of the PPSX000 HET. The experimental data show that the first and bigger peak corresponds to either a stationary or low velocity group of ions. This correspondence follows from a comparison between the first peak central frequency of a typical interference pattern and the central frequency of an interference pattern which is not Doppler shifted. To obtain an interference pattern that is not Doppler shifted, a FP measurement is performed at 90° with respect to the thruster axis aiming at the outer edge of the HET exit plane [10]. Thus, the axial velocity component is orthogonal to the line of sight and the ions have a negligible radial velocity component at this location. One then notices that the central frequency of the first peak of a typical interference pattern matches the central frequencies of a 'standing still' interfence pattern. Conversely, the second and smaller peak corresponds to groups of high-velocity ions. Note that signals obtained from other Xe^+ emission lines (λ = 460.30, 484.43, 529.22, and 533.93 nm) and with various thruster types display the same shape. More importantly, velocities calculated from interference patterns that correspond to different Xe^+ lines are the same. Therefore, the shape displayed in figure 2 is typical of FP measurements in the plasma of a HET. However, the shape of the measured signal is still not straightforward to interpret, so a theoretical model is used to extract accurate data from the measurements.

3. Data extraction

The shapes of the interference patterns originate in the integration of the plasma emissivity ε along the line of sight [10]:

$$I(\nu) = \int_{-\infty}^{+\infty}\int_{-\infty}^{+\infty}\int_{-\infty}^{+\infty} \varepsilon(\nu, \boldsymbol{r}) \cdot \mathrm{d}V, \tag{1}$$

$$\varepsilon(\nu, \boldsymbol{r}) = \frac{A}{2 \cdot \pi} \cdot n(\boldsymbol{r}) \cdot P(\nu, \boldsymbol{r}), \tag{2}$$

where A is the Einstein spontaneous emission coefficient, I is the signal intensity, $\boldsymbol{r}$ is the vector that locates the elementary volume $\mathrm{d}V$, ν is the light frequency, n is the number density of Xe^+ ions in the excited state from which collected light is emitted, i.e. n is the so-called emitter density, and P is the considered transition line shape.

The existence of nine stable Xe isotopes makes it difficult to study the 541.9 nm Xe^+ line, since the isotopic shifts and lower state hyperfine structure constants are unknown. However, since the FP interferometer resolution is $\sim$ 1 GHz and the atomic gas temperature T is about 800 K in a HET [8], it is possible to determine that the corresponding Doppler broadening is $\sim$0.64 GHz, whereas the natural line width of a single component is $\sim$0.01 GHz. Thus, we assume that the transition line shape P is approximated by a Gaussian function since Doppler enlargement dominates broadening processes in spite of the Zeeman effect. Indeed, we do not expect a strong impact of the magnetic field ($B < 150$ G) on the transition outside the channel [8]:

$$P(\nu, \boldsymbol{r}) \propto \frac{1}{\Delta\nu_D(\boldsymbol{r})} \cdot \exp\left(-4 \cdot \ln(2) \cdot \left(\frac{\nu - \delta\nu_D(\boldsymbol{r})}{\Delta\nu_D(\boldsymbol{r})}\right)^2\right), \tag{3}$$

$$\text{with } \delta\nu_D = \frac{1}{2 \cdot \pi} \cdot \boldsymbol{k} \cdot \boldsymbol{v} = \frac{v_z \cdot \nu_0}{c} \cdot \cos(\theta), \tag{4}$$

$$\text{and } \Delta\nu_D = 7.162 \times 10^{-7} \cdot \nu_0 \cdot \sqrt{\frac{T}{m_{Xe}}}, \tag{5}$$

where $\boldsymbol{k}$ is the wave vector, $\boldsymbol{v}$ is the Xe^+ ion velocity vector, v_z is the axial velocity component, ν_0 is the transition centre frequency, c is the speed of light, T is the gas temperature in K, and m_{Xe} is Xe atomic mass (in amu).

Therefore, an interference pattern contains information about the ion density, temperature through Doppler broadening $\Delta\nu_D$ and velocity through Doppler shift $\delta\nu_D$. Measurements show that the detection branch is far enough from the thruster so that the field depth may be considered infinite. Moreover, we have also assumed that the Xe plasma is fully transparent at 541.9 nm.

The sheer number of data contained in a FP interference pattern in addition to the fact that information is integrated in space makes it very difficult to determine the velocities of the different ion groups present along the line of sight. Therefore, a model is developed to allow data extraction [11]. Since a HET displays a cylindrical geometry, the problem is reduced to two dimensions. First, the detection branch is modelled to account for lens focal length, optical fibre diameter and the angle between the thruster axis and the line of sight. Second, modelling the HET plasma is trickier since it is initially unknown. The velocity distribution model assumes that the plasma plume is an expanding jet, which is a good approximation in the vicinity of the thruster channel axis according to numerical simulations of a hybrid model [12]. Finally, a FP interferometer measurement can be modelled through equations 3–5. However, the shape of the resulting

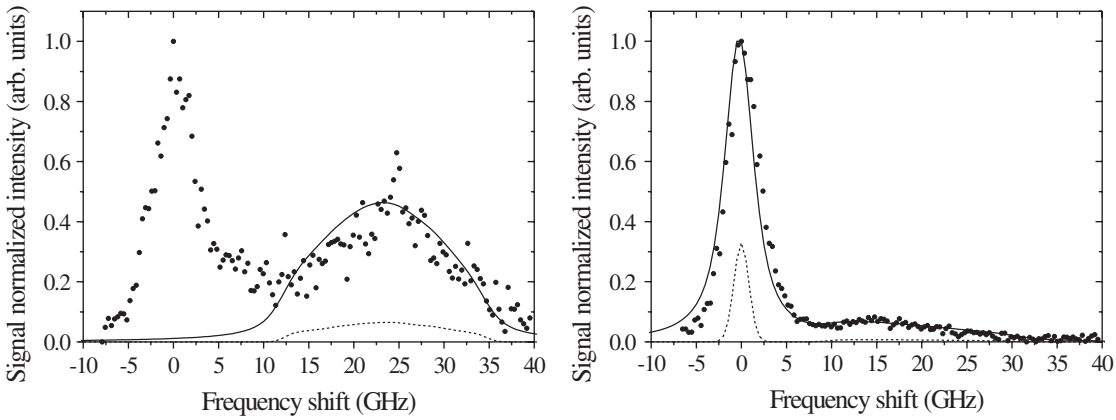

Figure 3. Calculated interference patterns convoluted (——) and not convoluted (- - - -) with the apparatus function compared with experimental measurements (· · · · · ·). Left curves: line of sight position = 20 mm, slow ions are not included in the simulation. Right curves: line of sight position = 2 mm, slow ions are included in the simulation. Thruster parameters: $U_d = 550$ V, and $\phi_a = 8.6$ mg s^{-1}.

interference pattern is highly sensitive to the spatial distribution of Xe^+ excited state density. In order to avoid using the outcomes of the existing hybrid model, which relies on a set of assumptions, a CCD camera is used at each operating condition so that a measured emitter density map can be extracted through the Abel transform of the corresponding pictures [11]. No narrow bandwidth optical filter is used in front of the CCD camera in order to collect all photons emitted within the emission line spectral profile. As a consequence the light intensity measurement images the Xe^+ excited state density in the collection volume. Moreover, the plasma medium is assumed to be optically thin in the visible range and non-radiative de-excitation by collisions are neglected. These two assumptions are reasonable under our experimental conditions. Because a CCD picture contains no data about the interior of the channel, the model is only valid if the line of sight does not intercept the HET channel.

Such a model provides realistic simulations for FP interference patterns, except for the amplitude of the first and higher peak of the figures, as can be seen in figure 3. Experiments show that the Doppler shift of this first peak falls below the FP interferometer resolution, meaning the corresponding velocity is below 0.5 km s^{-1} [8], as explained in section 2. Since the production mechanisms of these very slow, if not stationary, ions are still unknown, the total low velocity ion density for a given line of sight is arbitrarily set so that the simulations match the experimental interference patterns. Of course, the density map provided by the Abel transform of the CCD picture includes these slow ions, but calculations only include ions located in the expanding jet whose divergence is typically set at 30 °, i.e. the Abel transform of the CCD picture is not wholly used in the simulations. It is not possible that slow ions are located in the area of the maximum of electric field, i.e. in front of the channel, for they would be accelerated by the local electric field otherwise. Indeed, if such was the case, the ion velocity dispersion would be greatly increased. Then, even though the observed interference patterns would still present a peak at $v = 0$ m s^{-1}, it would also present a significant fast wing. In other words, we are confident that the density attributed to accelerated ions in the model does not correspond to slow ions. Comparisons between measured interference patterns and their simulated counterparts are displayed in figure 3. Note that the model takes the apparatus function of the FP interferometer into account [10]. Experimental and theoretical interference patterns match quite well, in spite of small discrepancies which can be explained by the over-simplistic approach of the plasma plume modelling.

The assumption that the centre of the second peak of the measured interference patterns corresponds to the ion velocity group whose density is the greatest, as identified on the Abel transform of the CCD picture, allows one to extract a velocity profile from a set of interference patterns [10]. In other words, each measured Doppler shift is assigned to a position on a two-dimensional density map, i.e. a CCD picture of the thruster. The Doppler shift is obtained by using the low velocity ion peak as a reference for null Doppler shift. This method of data extraction is correct if density and velocity gradients are steep enough, as suggested by outcomes of numerical simulations carried out with a hybrid model. Furthermore, the model described above allows one to check the validity of this assumption, provided that a CCD picture of the thruster for the corresponding parameters is available.

Note that the studied line corresponds to singly-charged ions. Therefore, doubly and triply-charged ions are not taken into account in this study, though it is well known that they are present in a HET plasma plume. However, singly-charged ions are mainly responsible for the thrust.

4. Results interpretation

4.1. Velocity profiles

Before reviewing results obtained with the PPSX000 thruster, it is of relevance to provide a validation of the experimental approach through comparison with the LIF diagnostic technique. The results of the comparison are summarized in figure 4. They were obtained during two measurement campaigns with a laboratory version of a SPT100 HET operating under optimal conditions [13, 14]. In the first case that corresponds to the left graph in figure 4, the ion velocity is directly inferred from the measured Doppler shift and ions are assumed to be located at the point of intersection between the line of sight and the channel axis [10]. The LIF velocity profile then permits one to move the FP velocity profile in the axial

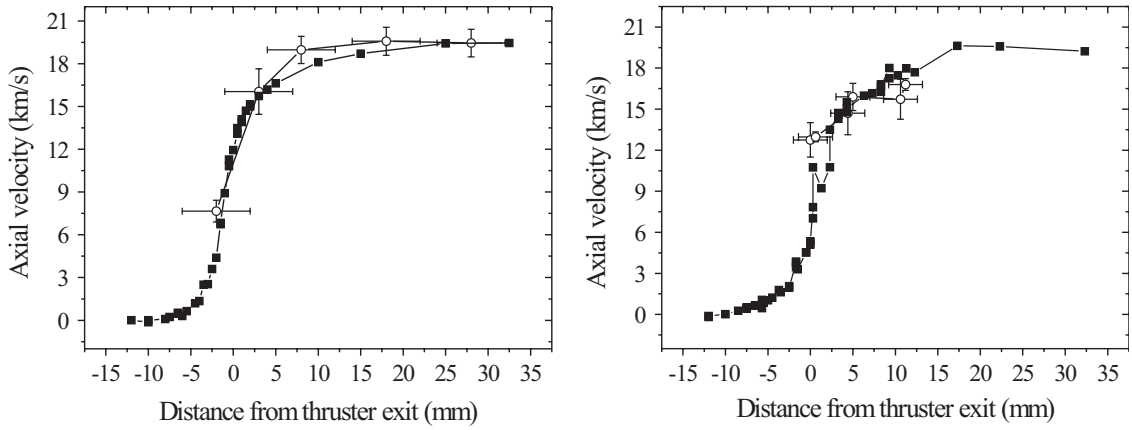

Figure 4. Comparison between axial ion velocity profiles measured by LIF spectroscopy (□) and FP interferometry (○) with a SPT100 thuster under optimal operating conditions. To the left: the velocity is directly calculated from the measured Doppler shift and the FP velocity profile is moved in space so that it matches the profile measured by LIF. To the right: The method described in this paper is used. The good agreement between FP and LIF data is obtained without repositioning any profile and error bars in axial direction are small.

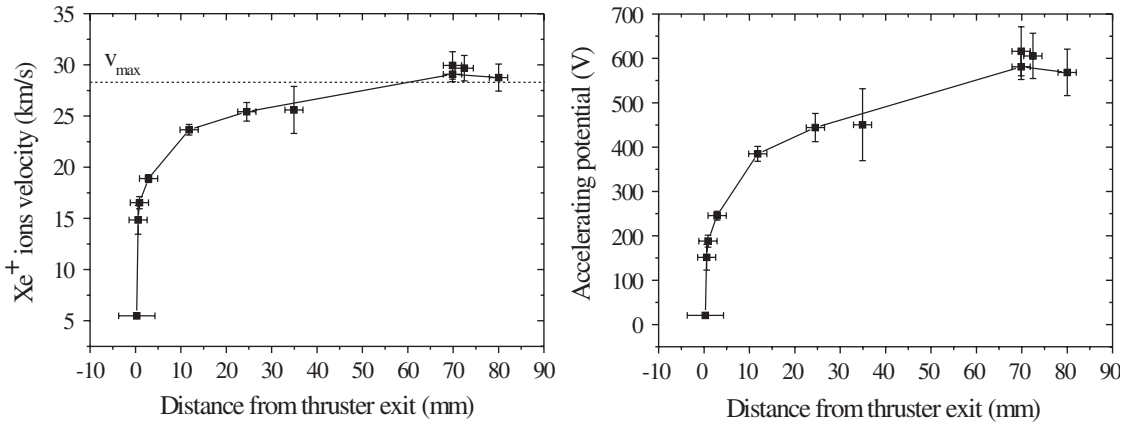

Figure 5. To the left: Xe^+ ion velocity profile (- - - - represents the maximum velocity that can be reached by the ions). To the right: accelerating potential seen by the Xe^+ ions. Thruster parameters for both curves: $U_d = 550\,V$ and $\phi_a = 8.6\ mg\,s^{-1}$.

direction [13]. In the second case (right graph), the approach described in this paper is followed: the FP velocity profile does not need to be shifted in space and error bars in axial direction are small [14].

The primary goal of FP measurements is to determine the evolution of the ion velocity as a function of distance from the thruster exit. The numerical model allows one to obtain such velocity profiles by assuming that the ion velocity is mainly axial near the channel centre line [12]. The velocity error bars in figures 5 and 6 are standard deviation resulting from a series of measurements, whereas the distance error bars are estimated through the numerical model. The distance uncertainty is estimated at ∼2 mm, which is the experimental resolution. Even though it may seem surprising that the experimental spatial resolution should be better than the width of the line of sight, one has to take the steep velocity and density gradients into account. These steep gradients ensure that the ion velocity group whose density is the greatest is the most visible on the interference pattern, in spite of several other ion groups. Note that the profile point at 0 mm, i.e. at the thruster channel exit, displays a more important error bar because it is difficult to determine whether this point is really located at the thruster exit or inside the thruster channel. Indeed, a small part of the line of sight does intercept the thruster channel at this position. Therefore, this position is at the boundary of the model validity domain.

In the rest of the paper, the accelerating potential U_{acc} seen by Xe^+ ions is calculated from the velocity profile by making the assumption that there is no energy transfer through collisions:

$$U_{acc} = \frac{1}{2 \cdot e} \cdot m_{Xe} \cdot v^2, \tag{6}$$

where e is the electron charge, m_{Xe} is Xe atom mass and v is the ion velocity. In the case of a HET, the local potential calculated using equation 6 does not correspond to the real accelerating potential an ion created far upstream experiences due to partial overlap between ionization and acceleration regions. Indeed, ions produced in the acceleration layer achieve a peak velocity below the hightest one. Nevertheless, the potential profile obtained in this way gives a good assessment of the real potential fall near the thruster exhaust [14].

Obtained velocity profiles are similar to what has already been observed in the past with other thrusters [10]. Ion acceleration occurs mainly outside the thruster channel and velocity gradients are very steep, which means the electric field created by the confinement of electrons is well localized

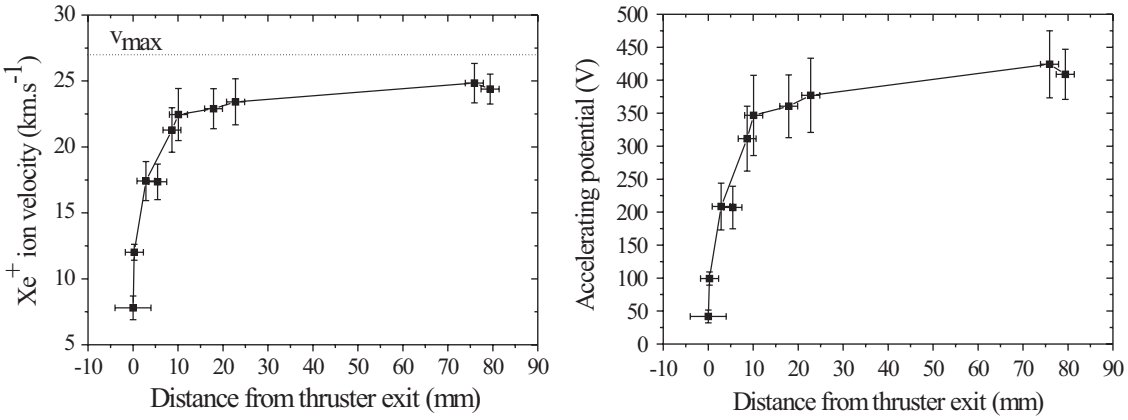

Figure 6. To the left: Xe^+ ion velocity profile (- - - - represents the maximum velocity that can be reached by the ions). To the right: accelerating potential seen by the Xe^+ ions. Thruster parameters for both curves: $U_d = 500$ V, and $\phi_a = 6$ mg s^{-1}.

and strong. Note that the v_{max} value indicated in figures 5 and 6 correspond to the velocity that ions could reach if all the discharge energy was transmitted to them:

$$v_{max} = \sqrt{\frac{2 \cdot e \cdot U_d}{m_{Xe}}} \tag{7}$$

The fact that ion velocity is close to v_{max} far from the thruster exit proves the efficiency of the PPSX000, even when taking the uncertainties of the data extraction method into account.

As can be seen in figures 5 and 6, the ion velocity profiles display two regimes, a steep gradient one near the thruster channel exit and a weak gradient one a few millimeters away from the channel, which translate into almost linear regimes for the accelerating potential. In a HET the acceleration mostly occurs ahead of the channel exhaust, a region where both electric and magnetic fields are strong. The acceleration is less and less pronounced as the potential reaches its limit set by the applied voltage and plasma conditions. The potential distribution merely originates in the development of the electron mobility in axial direction. The border between the two regimes, high and low acceleration degree, occurs outside the thruster channel and its location depends on the operating conditions, or in other words on the shape of the axial electric field profile. Until now, the hybrid model developed at CPAT relies on the assumption that the geometric discontinuity caused by the thruster channel represents a natural border to distinguish between two electron mobility regimes [15]. Inside the thruster channel, the 'anomalous' electron mobility is proportional to $1/B^2$, B being the magnetic field, as electron-wall collisions are expected to drive the electron properties. Outside the thruster channel, a turbulent electric field is assumed to cause the 'anomalous' electron mobility, which is then proportional to $1/B$. In view of the outcomes of this work, we suggest to fixing in the HET hybrid model the border between the two mobility regimes in the thruster channel near field. The criterion needed to set the location of the border is still to be defined; however, it could be based on magnetic field magnitude or gradient. This empirical approach is strengthened by the fact that all LIF spectroscopy measurements show that the channel exit plane is not a boundary in terms of accelerating potential as there is no sudden change in the potential profile at this location. Note that

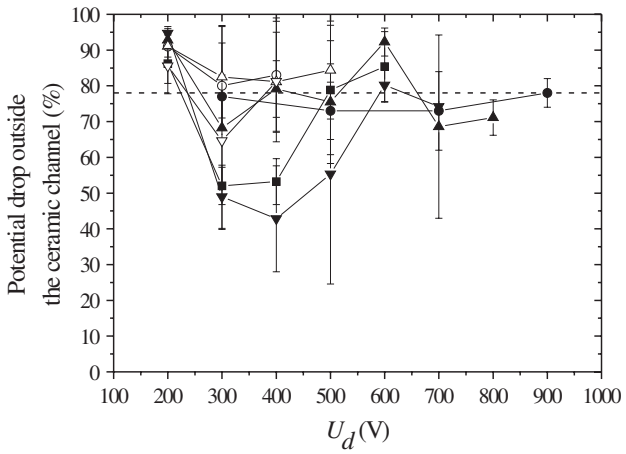

Figure 7. Potential drop outside the thruster channel as a function of U_d for different mass flow rates: $\phi_a = 5$ mg s^{-1} (●), $\phi_a = 6$ mg s^{-1} (■), $\phi_a = 8$ mg s^{-1} (▲), $\phi_a = 11$ mg s^{-1} (□) and $\phi_a = 15$ mg s^{-1} (○).

this approach suggests using Bohm mobility both inside and outside the thruster channel. An extensive discussion about modelling of anomalous electron mobility can be found in [16].

Furthermore, it has been possible to show that the potential drop seen by the Xe^+ ions occurs mainly outside the thruster. To this end, the PPS X000 HET has been operated over a wide range of operating conditions: discharge voltages of 200 to 900 V and Xe mass flow rates of 5 to 15 mg s^{-1}, which corresponds to a power range of 2 to 6 kW. In each case the magnetic configuration is optimized to minimize the discharge current I_d. For each set of parameters, two interference patterns are measured; the first corresponds to a line of sight intercepting the inside of the thruster channel, whereas the second interference pattern corresponds to a line of sight intercepting the plasma plume far downstream where the ion velocity is constant. These two values of the ion velocity are used to estimate the percentage of U_{acc} that occurs outside the thruster channel. As can be seen in figure. 7, the potential drop typically occurs at ~70% outside the thruster channel, even though it has not been possible to highlight tendencies in the evolution of this percentage with the thruster parameters. Complete velocity profiles are needed to reduce the error bars.

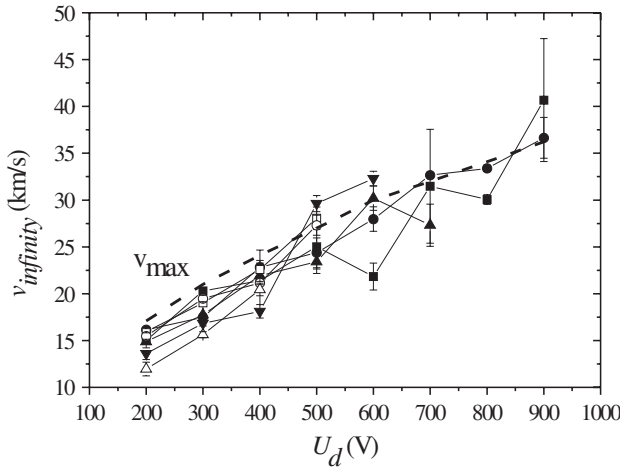

Figure 8. Ion velocity at 3 cm from the thruster exit (i.e. after the potential drop) as a function of U_d for different mass flow rates. (■: 5 mg s^{-1}; ●: 6 mg s^{-1}; ▲: 7 mg s^{-1}; ▽: 8 mg s^{-1}; □: 9 mg s^{-1}; ○: 11 mg s^{-1}; △: 15 mg s^{-1}).

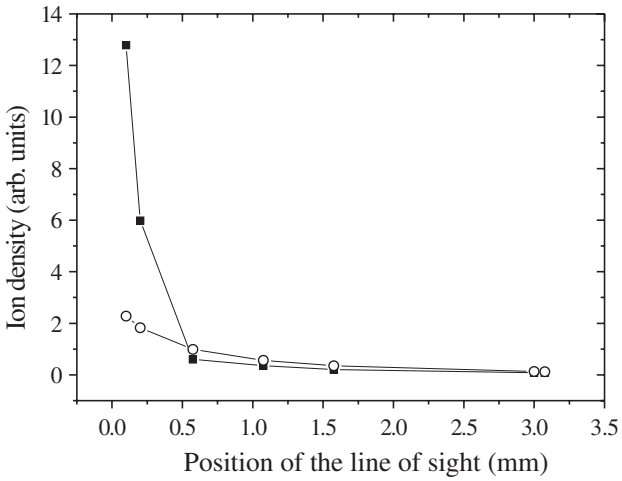

Figure 9. Slow ion density (□) and fast ion density (○) as a function of the position z of the line of sight.

Figure 8 displays the maximum ion velocity under different regimes, as well as the theoretical v_{max}. Even though the experimental curves roughly follow the trend of v_{max}, the changes introduced by a varying mass flow rate are quite sensitive. It is unclear why some working conditions lead to a lesser thruster efficiency, i.e. lower ion velocity far from the thruster exit. No obvious trend arises from the study of the influence of U_d and Xe mass flow rate on the thruster efficiency, even though the efficiency drops at high mass flow rate. Of course, elastic scattering increases with Xe mass flow rate, changing the distribution of the ion energy between the axial and radial velocity components, resulting in a decrease in the thruster efficiency. However, an ion energy of ∼150 eV yields to a elastic collision cross section of $\sim 1 \times 10^{-18}$ m^2 [17]. Thus, an atom density of $\sim 5 \times 10^{18}$ m^{-3} leads to an ion mean free path of ∼20 cm in the near field, which makes the influence of elastic scattering negligible. However, further measurements for mass flow rates between 9 and 20 mg s^{-1} should be performed before conclusions can be drawn. Note that some points above v_{max} show the limits of the FP diagnostic tool.

4.2. Slow ions

As already mentioned, a striking outcome of these measurements is that the contribution of slow ions to the FP line shape is significant. They may be created by charge exchange collisions between fast Xe^+ ions and slow Xe atoms or more likely by electron impact. Indeed, an ion energy of ∼200 eV yields a charge exchange cross section of $\sim 57 \times 10^{-19}$ m^2 [18]. Thus, an atom density of $\sim 5 \times 10^{18}$ m^{-3} yields an ion mean free path of ∼35 cm, which makes the charge exchange effect negligible. In order to locate these slow ions, it is possible to use the measured interference patterns as ion velocity distributions since the upper state of the 6p $^4D_{5/2} \longrightarrow$ 6s $^4P_{3/2}$ transition is equal to 9.5 ns, which means the velocity distributions are not deformed. Indeed, an ion with a velocity of 37 km s^{-1}, which is the maximum velocity theoretically reachable by ions when $U_d = 1000$ V, would take 194 ns to cross the FP volume of detection, so we can consider that every ion (be it fast or slow) has enough time to de-excite before leaving the line of sight. Of course, it also means an ion could be excited several times during a FP measurement. However, before an interference pattern can be used as a velocity distribution function, it should be deconvoluted by the FP interferometer apparatus function. Since a better signal-to-noise ratio is necessary, we chose to use the simulated interference patterns, which match the measured ones when they are convoluted by the FP apparatus function. These are the dashed lines shown in figure 3.

Slow and fast ion density can be estimated through the areas of the simulated interference patterns peaks. From figure 9, it is possible to see that the density of slow ions decreases drastically as the line of sight is moved away from the thruster exit. Thus near the thruster exit, when the line of sight is moved by 2 mm, i.e. less than the width of the line of sight, the density of slow ions decreases by ∼45%, whereas the density of accelerated ions stays roughly the same. Similarly, when the line of sight is moved by 7.4 mm away from the thruster exit, the slow ions density drops by more than 90%. Therefore, the slow ions are mainly produced and located near the thruster exit. This assertion is confirmed by the fact that the thruster pole is worn, which only occurs through ion bombardment. Theory does not explain why ions would be present in this area, but we can assume a weak or inverted electric field could trap ions. Slow ion production may not be important. Indeed, their low velocity ensures the corresponding flux is much lower than that of fast ions. Note that slow ions are necessarily produced in the area of the thruster pole, i.e. near the thruster axis, since they would see an electrical field that would accelerate them otherwise, hence leading to a positive flux. Yet, since slow ion density distribution is centred around 0 km s^{-1}, so is slow ion flux, meaning there is a negative slow ion flux.

Slow ions are not to be neglected since they may be responsible for cathode and pole erosion, plume divergence and interactions with spacecraft, hence decreasing the thruster efficiency and lifetime.

5. Conclusion

A non-intrusive and easy to implement diagnostic tool made of a FP interferometer, a CCD camera and a two-dimensional numerical model, has verified the presence of low velocity ions near the thruster exit in the plasma of a HET. Furthermore, the data show that the potential drop necessary to HET operation occurs mainly outside the thruster channel, which allows one to limit erosion. Keys to a better understanding of the 'anomalous' mechanisms of cross-field electron transport have also been highlighted.

Acknowledgments

The authors acknowledge the contribution of P Lasgorceix and the technical support of C Legentil, P Dom and S Sayamath. They would also like to thank M Touzeau and D Pagnon from LPGP who made the FP interferometry measurements possible.

This work has been carried out in the frame of the research group CNRS/CNES/SNECMA/Universités 2759 *'Propulsion Spatiale à Plasma'*.

References

[1] Racca G D 2004 *Proc. 4th Int. Spacecraft Propulsion Conf. (Sardinia, Italy)* (Noordwijk, ESA Publications Division)
[2] Kim V, Kozlov V, Lazurenko A, Popov G, Skrylnikov A, Clauss C, Day M and Sancovic J 1998 *34th AIAA Joint Propulsion Conf. Exhibit (Cleveland, OH, USA)* AIAA paper 98-3335
[3] Manzella D H, Jacobson D T and Jankovsky R S 2001 *Proc. 37th AIAA Joint Propulsion Conf. Exhibit (Salt Lake City, UT, USA)* AIAA paper 01-3774
[4] Koppel C R and Estublier D 2005 *Proc. 29th Int. Electric Propulsion Conf. (Princeton University, NJ, USA)* paper 119
[5] Duchemin O and Dumazert P 2003 *Proc. 28th Int. Electric Propulsion Conf. (Toulouse, France)* paper 0032
[6] Meulenbroeks R F G, van der Heijden P A A, van de Sanden M C M and Schram D C 1994 *J. Appl. Phys.* **75** 2775
[7] Timmermans C J, Lunk A and Schram D C 1981 *Contrib. Plasma Phys.* **21** 117
[8] Mazouffre S, Pagnon D, Lasgorceix P and Touzeau M 2003 *Proc. 28th Int. Electric Propulsion Conf. (Toulouse, France)* paper 283
[9] Hofer R, Peterson P and Gallimore A 2001 *Proc. 27th Int. Electric Propulsion Conf. (Pasadena, CA, USA)* paper AIAA-01-045
[10] Mazouffre S, Pagnon D and Bonnet J 2004 *Proc. 40th AIAA Joint Propulsion Conf. Exhibit (Fort Lauderdale, FL, USA)* AIAA paper 04-3949
[11] Gawron D, Mazouffre S and Boniface C 2005 *Proc. 29th Int. Electric Propulsion Conf. (Princeton University, NJ, USA)* paper 144
[12] Hagelaar G J M, Bareilles J, Guarrigues L and Boeuf J-P 2002 *J. Appl. Phys.* **91** 5592–8
[13] Dorval N, Bonnet J, Marque J P, Rosencher E, Chable S, Rogier F and Lasgorceix P 2002 *J. Appl. Phys.* **91** 4811–17
[14] Gawron D, Mazouffre S, Albarède L and Sadeghi N 2006 *Proc. 42nd AIAA Joint Propulsion Conf. Exhibit (Sacramento, CA, USA)* AIAA paper 06-4473
[15] Hagelaar G J M, Bareilles J, Garrigues L and Boeuf J-P 2003 *J. Appl. Phys.* **93** 67–75
[16] Koo J W and Boyd I D 2006 *Phys. Pasmas* **13** 033501
[17] De Urquijo J *et al* 2000 *Proc. 53rd Gaseous Electronics Conf. (Houston, TX, USA)*
[18] Miller J S, Pullins S, Levandier D, Chiu Y-h and Dressler R 2002 *J. Appl. Phys.* **91** 984–91